CrossMark

Effects of Process Parameters on the Characteristics of Mixed-Halide Perovskite Solar Cells Fabricated by One-Step and Two-Step Sequential Coating

Mohammad Reza Ahmadian-Yazdi, Fatemeh Zabihi, Mehran Habibi and Morteza Eslamian[*]

Abstract

In this paper, two-step sequential spin-dip and spin-spin coating, as well as one-step spin coating, methods are used to fabricate methylammonium lead mixed-halide perovskites to study the effect of process parameters, including the choice of the solvent, annealing temperature, spin velocity, and dipping time on the characteristics of the perovskite film. Our results show that using a mixture of DMF and DMSO, with volume ratio of 1:1, as the organic solvents for $PbCl_2$ results in the best mixed-halide perovskite because of the effective coordination between DMSO and $PbCl_2$. Surface dewetting due to two effects, i.e., crystallization and thin liquid film instability, is observed and discussed, where an intermediate spin velocity of about 4000 rpm is found suitable to suppress dewetting. The perovskite film fabricated using the one-step method followed by anti-solvent treatment shows the best perovskite conversion in XRD patterns, and the planar device fabricated using the same method exhibited the highest efficiency among the employed methods. The perovskite layer made by sequential spin-dip coating is found thicker with higher absorbance, but the device shows a lower efficiency because of the challenges associated with perovskite conversion in the sequential method. The one-step deposition method is found easier to control and more promising than the sequential deposition methods.

Keywords: Photovoltaics, Mixed-halide perovskite, Sequential deposition, Crystallization dewetting, One-step deposition

Background

Lead halide perovskite solar cells have drawn enormous attention due to their rapid rise in device power conversion efficiency (PCE), only within a few years, now hitting a record PCE of 22 % achieved by Seok's group (KRICT/UNIST, South Korea), although the device was not stabilized [1]. The perovskite crystal structure has the chemical formula of ABX_3, where in the perovskite molecule used in solar cells as the light-harvesting layer, A is usually methylammonium, B is lead, and X is a halogen or a mixture of several halogens, thus making the $CH_3NH_3PbX_3$ molecule with proper light absorbance and bandgap suitable for photovoltaic applications [2, 3]. Miyasaka was the first who employed it as a sensitizer layer in dye-sensitized solar cells and achieved a PCE of 3.8 % [4]. Since then, attempts have been made to engineer the device structure to increase the efficiency and stability [5]. Methylammonium lead halide perovskite usually forms according to the following chemical reaction between its two precursors:

$$PbX_2 + CH_3NH_3X \xrightarrow{\text{Organic solvents, Temp.}} CH_3NH_3PbX_3 \quad (1)$$
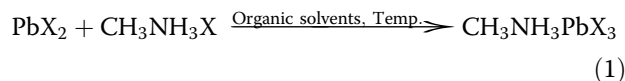
where X is a halogen, usually I or Cl, which could be the same in both precursors or different. Both the single-halide $CH_3NH_3PbI_3$ and mixed-halide $CH_3NH_3PbI_{3-x}Cl_x$ perovskite molecules have been widely used as the light-harvesting layer in perovskite solar cells (SCs) [6]. However, it has been demonstrated that the mixed-halide perovskite exhibits superior photovoltaic performance,

* Correspondence: Morteza.Eslamian@sjtu.edu.cn; Morteza.Eslamian@gmail.com
University of Michigan-Shanghai Jiao Tong University Joint Institute, Shanghai 200240, China

Ahmadian-Yazdi *et al. Nanoscale Research Letters* (2016) 11:408

Page 2 of 11

such as small exciton binding energy [7], high charge-carrier mobility, and large exciton diffusion length over 1 μm, which makes it compatible with various cell structures. Compared to $CH_3NH_3PbI_3$, the chlorine ion in mixed-halide perovskite $CH_3NH_3PbI_{3-x}Cl_x$ improves the charge-carrier transport [8, 9], the charge collection of the cell, and the band bending, and lowers the charge recombination rate. It is, however, difficult to tune the chemistry of the chlorine-doped perovskite, as it requires solvent engineering and well-controlled deposition methods. This entails more research on mixed-halide perovskites to understand the perovskite conversion process and the film characteristics.

Given that perovskite has a crystalline structure, thin layers of perovskite used in solar cells are prone to dewetting because of the growth of rather large crystals on the film, adversely affecting the film intactness and coverage. Significant progress has been made in the film morphology and surface coverage; however, the perovskite films still suffer from rough and non-uniform morphologies [10], indicating the need for more studies to understand the process and to obtain pinhole-free films.

As Eq. (1) suggests, the perovskite can be fabricated using a wet chemistry process. The first solution-processed perovskite layer (CH_3NH_3PbI) was synthesized on a mesoporous TiO_2 scaffold and incorporated into an electron/hole-selective-free device [4]. The mesoporous scaffold made of nanoparticles of TiO_2 helps in the controlled growth of perovskite crystals. The mesoporous scaffold filled with perovskite crystals also helps in the effective charge collection in a short distance, which is within the diffusion length of the charges. This structure was then developed by addition of electron- and hole-transporting layers and replacing the TiO_2 scaffold by other ceramics, such as Al_2O_3. These mesoporous 3D structures are known as the typical structure for perovskite SCs, but they essentially need high process temperatures for their fabrication, hindering low-cost fabrication of perovskite SCs, especially on flexible plastic substrates. To suppress the difficulties associated with mesoporous structures, an alternative structure has been suggested, based on deposition of perovskite reagents on flat substrates, called planar or 2D structure [11]. The planar structure is better matched with the properties of the mixed-halide perovskites, which possess longer charge diffusion lengths compared to single-halide perovskites. Planar perovskite devices can be fully processed in solution and deposited using a casting method. However, in a planar structure, the elimination of the mesoporous scaffold, which functions as a template for crystal growth, complicates the controlled deposition, chemical conversion, crystal growth orientation, and may cause hysteresis at the interfaces. To suppress these difficulties, several attempts have been made to control the crystal growth and improve the

interfaces of perovskite with the adjacent layers by employing various deposition methods, such as vapor deposition or solution-processed casting methods, e.g., [11–19]. The deposition method affects the characteristics of the resulting thin films, i.e., the coverage, thickness, roughness, and therefore the light-harvesting and charge-carrier pathways. Perovskite layers may be deposited sequentially in two steps, given that two precursors are involved in the fabrication of perovskite (Eq. 1), or in one step, by mixing and depositing the precursors. Each approach has its advantages and disadvantages. For instance, although some works indicate the supremacy of the sequential deposition, other studies reveal that the perovskite thin film deposited on a flat substrate may result in incomplete conversion of precursors to perovskite [20], due to inadequate mixing of precursors in the sequential deposition.

Regardless of the fabrication route, understating and controlling the process parameters, such as annealing temperature, concentration of precursors, and employed solvents and additives, play critical roles in the film surface quality, coverage, conversion of precursors to perovskite, crystallinity, crystal size, and therefore the performance of the layer and the entire device [21]. Following the forgoing introduction, the main goal of this work is to understand the effect of the aforementioned parameters on perovskite film and device performance. The planar structure is adopted for its low-temperature processing, and the mixed-halide perovskite is chosen for its better performance, longer charge diffusion length, and compatibility with planar structure. By varying several process parameters, we attempt to obtain the optimum conditions. Three fabrication routes are followed to make perovskite layers: two-step sequential spin-dip and spin-spin coating and one-step spin coating. The solar cells, made based on the optimum condition, have a planar FTO-coated glass/c-TiO_2/perovskite/spiro-OMeTAD/Ag structure, where FTO denotes fluorine-doped tin oxide, c-TiO_2 denotes compact TiO_2 film, and spiro-OMeTAD is the short form for 2,2′,7,7′-tetrakis(*N*,*N*′-di-*p*-methoxyphenylamine)-9,9′-spirobifluorene.

Methods

Methylammonium iodide (MAI, 99.5 %) was supplied by Xia'an Reagents Co., China. 2-Propanol (IPA, anhydrous, 99.5 %), *N*,*N*-dimethyl formamide (DMF, 99.8 %, biological grade), chlorobenzene (CB, 99.9 %, analytical grade), dimethyl sulfoxide (DMSO, 99.5 %, biological grade), hydrogen chloride (HCl, 37.5 %), lead chloride ($PbCl_2$, 98.5 %), ethanol (99.9 %, biological grade), toluene (98.8 %), bis(trifluoromethane)sulfonamide lithium salt (99.95 %), acetonitrile (99.8 %), 4-tert-butylpyridine (96 %), and titanium (IV) isopropoxide (97 %) were purchased from Sigma-Aldrich, USA.

Fluorine-doped tin oxide (FTO)-coated glass (25 mm × 25 mm × 2.2 mm) was washed by detergent, deionized

Ahmadian-Yazdi *et al. Nanoscale Research Letters* (2016) 11:408

Page 3 of 11

water, and 2-propanol in an ultrasonic bath for 30 min, followed by UV-ozone treatment for 15 min. For the preparation of compact TiO_2 layer (c-TiO_2), as the electron-transporting layer (ETL), 350 μl of titanium isopropoxide solution was diluted in 5 ml of ethanol. Also, 32.5 μl of HCl (2 M) was diluted in 2 ml of ethanol. Then, the acidic solution was added to titanium isopropoxide solution dropwise, under stirring condition. The resultant solution was then cast by two methods: spray coating and spin coating at 2000 rpm for 60 s. The resulting thin films were annealed at 150 °C, for 30 min. The spray-on c-TiO_2 thin films were rough and demonstrated low device performance, when used for device fabrication, and therefore were discarded.

Perovskite thin films were prepared using one-step and also two-step sequential casting of precursor solutions: $PbCl_2$ was dissolved in DMF, DMSO, and a mixture of both solvents at various concentrations (c.f. Table 1), while MAI was dissolved in sufficient amount of IPA to obtain a concentration of 10 mg/ml. In order to investigate the influence of the choice of solvent on thin film quality and surface coverage and morphology of crystals, $PbCl_2$ was dissolved in various ratios of DMSO to DMF solvents. In the spin-dip two-step sequential coating, the $PbCl_2$ solution was spun for 60 s, at various spin speeds of 1000, 4000, and 7000 rpm. The resulting wet film was then heat-treated at 90 °C for several seconds and was immediately dipped into the MAI solution and kept for 90 or 150 s to study the effect of dipping time. As-spun thin films were annealed at various temperatures of 100 and 160 °C, for 30 min. In the spin-spin two-step sequential coating, the $PbCl_2$ film was made by the same method just described for the spin-dip process, and then, the MAI

solution was spun over at 2000 rpm for 40 s. Then, the wet film was heat-treated at 90 °C for 1 h. Due to the hygroscopic nature of MAI and instability of the $CH_3NH_3PbI_{3-x}Cl_x$ film in ambient conditions, all samples were fabricated in a nitrogen-filled glove box.

For the one-step deposition, the perovskite precursor solution was prepared by dissolving 481 mg of PbI_2, 40 mg of $PbCl_2$, and 100 mg of MAI in 1 ml of DMSO. The solution was spun for 20 s at 750 rpm and then immediately for 60 s at 3000 rpm. After 40 s, 300 μl of toluene was dropped onto the thin film and the obtained wet film was annealed at 100 °C for 10 min.

Devices were fabricated using the perovskite films made based on the two-step sequential spin-dip method at optimum process conditions (run 1 of Table 1), as well as the one-step method. To deposit the hole-transporting layer (HTL), 60 mg of spiro-OMeTAD, 480 mg/ml of lithium salt in acetonitrile, and 20 μl of 4-tert-butylpyridine were added to 1 ml of chlorobenzene and the solution was spun at 2000 rpm for 30 s. The wet film was kept for 12 h under nitrogen atmosphere. To complete the device, 200 nm of Ag was deposited by thermal evaporation. The active area of the cells made in this work is about 0.076 cm^2. To further improve the perovskite conversion of the optimum run 1 of spin-dip coating for X-ray diffraction (XRD) analysis and device fabrication, after spinning of $PbCl_2$, as mentioned above, a PbI_2 solution (10 mg/ml in DMSO) was spun over at 5000 for 30 s.

Surface topography of the perovskite thin films were characterized using a confocal laser scanning microscope (CLSM, model LMS700, Zeiss, Germany) and a scanning electron microscope (SEM, Hitachi, Model S-3400N,

Table 1 The list of experimental runs and variables used in this study. The measured roughness values of perovskite films are also listed

Run #	Concentration of $PbCl_2$ (mg/ml)	Annealing temp. (°C)	Spin velocity (rpm)	Dipping time (s)	DMSO vol. (ml)	DMF vol. (ml)	Roughness (μm)	Coating method
1[†]	200	100	4000	90	2	2	0.10	Spin-dip
2	200	160	4000	90	2	2	0.20	Spin-dip
3	200	100	7000	150	2	2	0.20	Spin-dip
4	200	100	1000	150	2	2	0.20	Spin-dip
5	200	100	4000	150	2	2	0.25	Spin-dip
6	267	100	4000	90	2	1	0.26	Spin-dip
7	267	100	1000	90	1	0	0.10	Spin-dip
8	150	100	4000	150	2	2	0.13	Spin-dip
9	150	100	4000	90	2	2	0.10	Spin-dip
10	200	100	4000[a] 2000[b]	–	2	2	0.67	Spin-spin
11[c]	–	100	–	–	0	1	0.20	One-step

[†]Run 1 was found to be the optimum case. For XRD device fabrication and XRD analysis, after deposition of $PbCl_2$, a layer of PbI_2 was also deposited to further improve the perovskite coverage and conversion, as outlined in the "Methods" section
[a]Spin velocity for deposition of $PbCl_2$ precursor
[b]Spin velocity for deposition of MAI precursor
[c]Details are given in the "Methods" section

Ahmadian-Yazdi *et al. Nanoscale Research Letters* (2016) 11:408

Page 4 of 11

Japan). The surface roughness was obtained using the CLSM over an area of 65 μm × 65 μm. A UV-vis spectrometer (Lambda 20, PerkinElmer Inc., USA) was used to obtain the absorbance spectra. XRD (model D5005, Bruker, Germany) was utilized to characterize the crystallographic patterns of thin films. Average perovskite particle (crystal) size was measured by Zetasizer (Malvern, nano-zs90). Interaction of DMSO and DMF solvents with $PbCl_2$ was analyzed using X-ray photoelectron spectrometry (XPS, Kratos, Axis ultra DLD). The device photovoltaic performance and the *J-V* curves were obtained using a solar simulator and a Keithley source meter, model 2450, the Netherlands, under AM1.5G solar irradiation at a power intensity of 100 mW/cm^2, in the range of 0 to +1 V bias.

Results and Discussion

Table 1 lists the process parameters, i.e., the annealing temperature, concentration of $PbCl_2$, type and ratio of the organic solvents used to dissolve $PbCl_2$, spin velocity, and the perovskite deposition method, as well as the roughness of the perovskite films, fabricated in a nitrogen-filled glove box. Most samples listed in Table 1 were made by the two-step sequential spin-dip coating, one sample listed was made by the two-step sequential spin-spin coating, and one sample was made by the one-step deposition. In the following sub-sections, using the data listed in Table 1 and proper figures, the effects of various process parameters on some characteristics of perovskite films are investigated.

Annealing is an important step performed after deposition of perovskite films, to tune the film crystallinity, to eliminate solvent residues, and to stabilize the perovskite structure. Here, we studied how temperature could affect the perovskite conversion and also distribution and uniformity of perovskite crystals. The laser images of perovskite films made by spin-dip coating using annealing temperatures of 100 and 160 °C (runs 1 and 2) are illustrated in Fig. 1a, b. Two different morphologies are observed. At higher temperature of 160 °C, perovskite crystals are apparently more uniformly distributed. Upon casting of the precursor solutions, an organic/halide-rich wet film forms, where the annealing process helps the excess organic and halide components evaporate, until a stoichiometric ratio of organic:metal:halide is reached [22]. At a higher annealing temperature, the evaporation rate is faster resulting in smaller and more uniform crystals because high evaporation rate arrests excessive crystal growth. However, it was observed that at annealing temperatures higher than 170 °C, the surface coverage decreases, due to aggregation or sintering of perovskite crystals in severe thermal conditions (data not shown). It was also inferred that annealing at very high temperatures results in degradation of perovskite, evidenced by appearing

shiny yellow color sites on the surface, indicating the formation of PbI_2 crystals. In agreement with this argument, Fig. 1c shows that annealing at 160 °C, compared to 100 °C, results in partial decomposition of perovskite. Therefore, overall, it is concluded that annealing at 100 °C is preferred and therefore used here for device fabrication.

The laser images of the films made at the conditions of runs 3, 4, and 5 to study the effect of spin velocity and therefore the film thickness on the overall film morphology are shown in Fig. 2, where surface features including pinholes can be observed. As the spin velocity increases, the liquid film thickness decreases, and if the liquid film becomes very thin (less than 100 nm or so), the intermolecular forces, such as van der Waals forces, between the liquid film interfaces (liquid-air and solid-liquid) become dominant and larger than the stabilizing gravity and capillary forces due to surface tension, and the film may become prone to spinodal dewetting, given that ultrathin films are usually metastable. In addition, a thin liquid film may partially break up and dewet the surface, due to heterogeneous nucleation, induced by the presence of impurities on the substrate or within the film. Such heterogeneous nucleation may be induced by thermal effects, as well [23]. Besides the conventional dewetting of thin liquid films that may occur due to the growth of perturbations, dewetting in evaporating thin films of liquid solutions may also occur due to crystallization dewetting, i.e., the formation of large crystals that consume the solid content, thus creating dewetted areas adjacent to the large crystals [24]. A thin liquid film of perovskite precursor solution is a perfect example that shows the occurrence of crystallization dewetting, due to the growth of large crystals of perovskite. In summary, at high spin speeds or low film thickness, the chance of dewetting due to crystallization as well as breakup due to excessive growth of liquid film perturbations increases, as observed clearly in Fig. 2c (7000 rpm) and partially in Fig. 2b (4000 rpm). In Fig. 2, the $PbCl_2$ solution was spun for 60 s. The relationship between the estimated film thickness and spin velocity and duration of spinning may be found in Ref. [23].

To promote perovskite conversion and to control the kinetics of crystal growth and to avoid dewetting, various approaches are employed, including solvent treatment. A strong coordination between the solvent and the solute is the determining factor for selection of a favorable solvent. A good coordination between the solvent and solute is beneficial for effective distribution of the solute in the solvent and therefore uniform crystallization and coverage of the film [25]. Also, the choice of the solvent usually affects the crystal size [24]. Most studies indicate that larger crystal size (e.g., those obtained by DMSO-based solution) favors the light absorbance, e.g., [26]. However, the large crystals tend to cause crystallization dewetting and adversely affect the film coverage, which
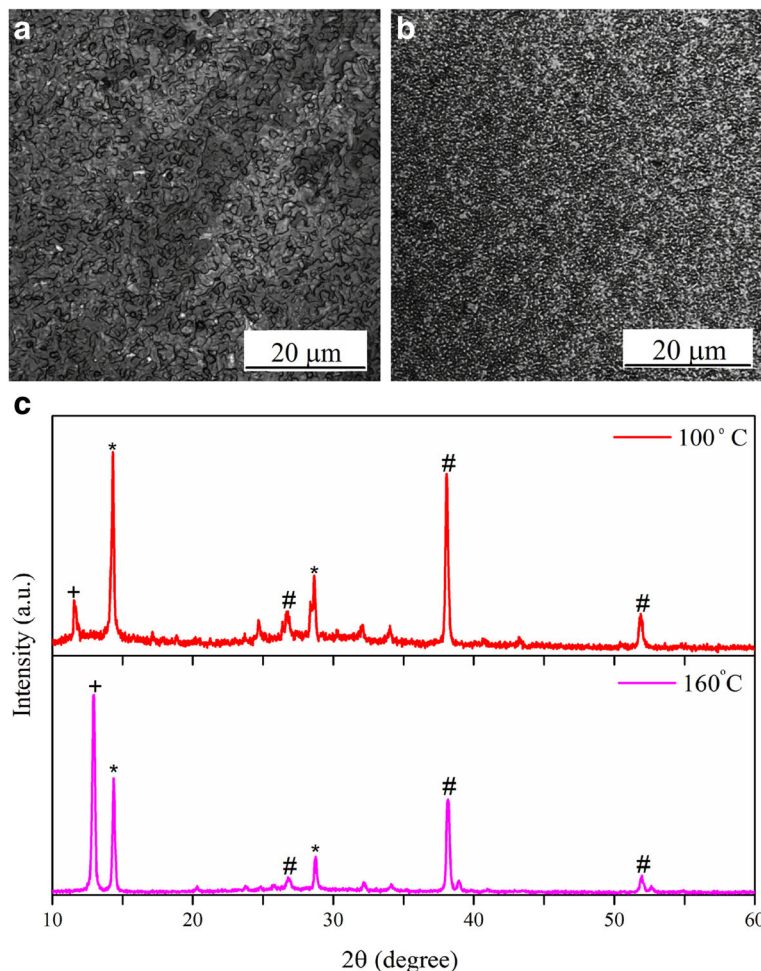
Ahmadian-Yazdi *et al. Nanoscale Research Letters* (2016) 11:408

Page 5 of 11

Fig. 1 Effect of annealing temperature: laser images of perovskite surface morphology, made using spin-dip coating at **a** annealing temperature of 100 °C (run 1) and **b** annealing temperature of 160 °C (run 2). The field of view is 65 μm × 65 μm. **c** The XRD patterns of perovskites annealed at 100 and 160 °C. The *asterisk* denotes the perovskite peaks, the *number sign* denotes the FTO peaks, and the *plus sign* denotes the PbI_2 peaks. Annealing at 100 °C is preferred because of better perovskite conversion and adequate coverage
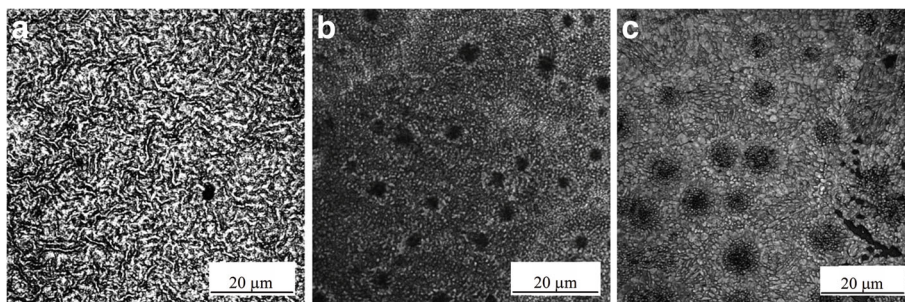

Fig. 2 Effect of spin velocity: laser images of spin-dip perovskites. The $PbCl_2$ films spun at **a** 1000 rpm (run 4), **b** 4000 rpm (run 5), and **c** 7000 rpm (run 3). All other process parameters were kept constant. The field of view is 65 μm × 65 μm

Ahmadian-Yazdi et al. Nanoscale Research Letters (2016) 11:408

Page 6 of 11

causes frequent shunt paths between perovskite and the adjacent layers. Here, the effect of using DMF and DMSO solvents on the coverage of perovskite thin films is investigated (Fig. 3). We found that DMF is a rather poor solvent for $PbCl_2$, whereas DMSO better dissolves $PbCl_2$. On the other hand, it has been shown that with DMF, perovskite formation occurs immediately after solvent evaporation, within a few minutes of annealing, while DMSO retards the reaction, because of the formation of strong DMSO-Pb-Cl- complexes [10, 13]. We speculated that using a mixture of DMF and DMSO would result in a controlled formation of perovskite and better coverage. Figure 3 shows the SEM images and crystal size distribution of perovskite layers made using DMSO and a mixture of DMSO and DMF solvents. The average perovskite crystal size and the size distribution were measured by a Malvern Zetasizer. Particle sizing is sometimes performed by analysis of SEM or optical images, but the particle sizer is more reliable and accurate. In image analysis, the image size and resolution may be

limited; it may be also difficult to recognize every individual grains, due to possible crystal agglomeration or overlapping in some samples. For particle sizing by Malvern Zetasizer, the whole sample is dispersed in a dispersant. Then, the crystals are separated or agglomerates are broken by agitation or sonication. Therefore, a large number of particles are subjected to particle counting. Figure 3d shows that the application of DMSO results in the formation of larger crystals compared to those made using DMF. As observed from the SEM images, the highest coverage is obtained when a mixture of DMSO and DMF with a volume ratio of 1 is employed (run 1). Also, the particle size distribution graphs (Fig. 3d) reveal that the application of the same mixture results in the formation of smaller crystals with a narrow size distribution compared with the case of using DMSO only. Application of a mixture of DMF and DMSO with a volume ratio of DMSO/DMF = 2 results in a bimodal size distribution with lower coverage. From a hydrodynamics point of view, addition of DMF to
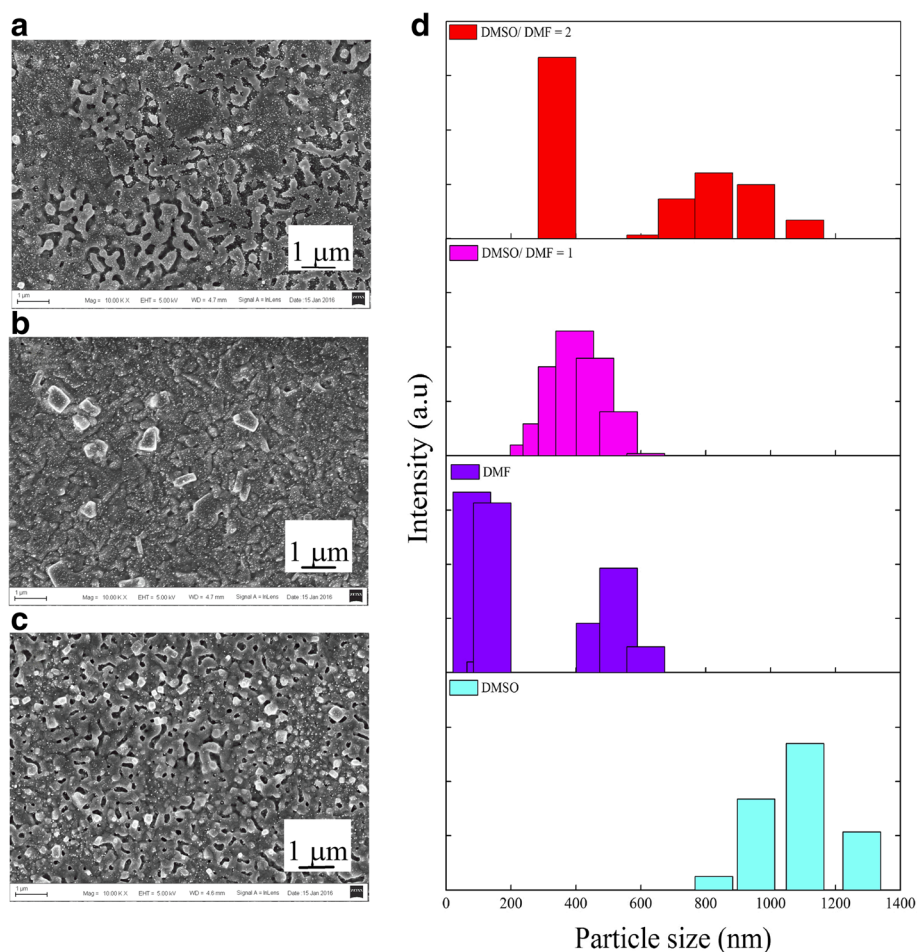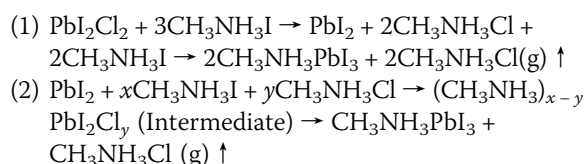

Fig. 3 Effect of the $PbCl_2$ solvent: SEM images of perovskite films made by spin-dip coating method, using various solvents for $PbCl_2$: **a** DMSO/DMF = 2 (run 6), **b** DMSO/DMF = 1 (run 1), **c** DMSO only (run 7), and **d** perovskite particle size distribution for various $PbCl_2$ solvents

Ahmadian-Yazdi *et al. Nanoscale Research Letters* (2016) 11:408

Page 7 of 11

DMSO increases the solution surface tension, thus improving the thin liquid film stability and uniform coverage of the resulting solid film. Besides, addition of DMF decreases the polarity of the solution. In the case of partial drying, a residual polar solvent may boost the hydration of perovskite crystals.

Literature reports show that strong coordinating solvents, such as DMSO, facilitate the formation of a uniform film of PbI_2 crystals [27, 28]; however, there is no report on the same effect on $PbCl_2$, and thus, it is studied here by XPS analysis, as shown in Fig. 4. In Fig. 4, the located high peaks at 138.7 and 143.5 eV are associated with $PbCl_2$ bonds [27]. As shown in Fig. 4, the $PbCl_2$ sample made using DMF has only two peaks associated with $PbCl_2$, whereas the sample made using a mixture of DMF and DMSO has an additional low-intensity Pb-O peak, since the polarity of DMSO is larger than that of DMF. Furthermore, because of the high polarity of DMSO, which is the result of the bond between S and O, DMSO can make covalent bonding with $PbCl_2$. This behavior of $PbCl_2$ in mixed DMSO/DMF solvent is similar to that of PbI_2, observed before by others, i.e. the PbI_2 is more uniform and homogenous in the solution, in the presence of both DMSO and DMF [27, 28]. With an increase in the volume of DMSO, the coordination of $PbCl_2$ with DMSO increases, which favors the formation of $PbCl_2$ clusters. Therefore, the crystals further grow, but excessive amount of DMSO may cause the formation of needle-shape crystals and a decrease in the coverage of the perovskite layer, as observed in the SEM images of Fig. 3.

Based on our preliminary experiments and the literature data, two reasonable dipping times of 90 and 150 s were selected in spin-dip experiments, to study its effect on the surface coverage and roughness. Increasing the dipping time of the $PbCl_2$ layer in the MAI solution, generally, provides longer time for conversion of

Fig. 4 XPS of $PbCl_2$ dissolved in different solvents

precursors to perovskite crystals. However, excessive exposure times may cause dissolution of the perovskite layer, leading to film deterioration or a decrease in coverage. Figure 5 shows the effect of dipping time on samples made at 4000 rpm and $PbCl_2$ concentration of 150 mg/ml for two different experimental conditions (runs 8 and 9). One observation made here is that the spin-dip perovskite made based on 90 s dipping time is more uniform and appears single-phase, whereas the sample made based on 150 s appears two-phase and affected by the excessive dipping time. Comparing run 8 ($t = 150$ s) with run 9 ($t = 90$ s) of Table 1 reveals that a longer dipping time results in a higher roughness. A higher roughness may translate to a larger crystal size. It is therefore concluded that within the range of the parameters studied here, the lower dipping time (90 s) is preferred. Furthermore, it has been inferred that in the formation of the mixed-halide perovskites, such as the current work, CH_3NH_3ICl forms as an intermediate component, which may convert to $CH_3NH_3PbI_3$ in a long contact time, as exhibited by the following chemical reactions [29]:

(1) $PbI_2Cl_2 + 3CH_3NH_3I \rightarrow PbI_2 + 2CH_3NH_3Cl + 2CH_3NH_3I \rightarrow 2CH_3NH_3PbI_3 + 2CH_3NH_3Cl(g) \uparrow$

(2) $PbI_2 + xCH_3NH_3I + yCH_3NH_3Cl \rightarrow (CH_3NH_3)_{x-y} PbI_2Cl_y$ (Intermediate) $\rightarrow CH_3NH_3PbI_3 + CH_3NH_3Cl$ (g) $\uparrow$

A long contact time between the spun $PbCl_2$ film and the MAI solution may lead to the formation of $CH_3NH_3PbI_3$, and therefore the release of the CH_3NH_3Cl gas. Therefore, the new phase observed in Fig. 5b may be due to the prolonged contact between the precursors, which might have led to the formation of $CH_3NH_3PbI_3$.

Spin-dip process usually leads to the formation of thicker perovskite films. Although the thicker layer of perovskite may lead to improved light absorption, the film thickness cannot exceed the charge diffusion length. Therefore, alternatively, spin-spin coating may be adopted, instead of spin-dip coating, to make thinner layers. In this method, the dipping process is simply replaced by a second spinning process to deposit a thin layer of MAI solution atop the $PbCl_2$ layer. Dynamic interaction and mixing between solid $PbCl_2$ and wet MAI layers, due to spinning, results in the formation of perovskite. Run 10 of Table 1 shows the conditions of the spin-spin sample, determined based on the literature data and our preliminary optimization process. In order to enable high solvent evaporation, the substrate was heated before precursor deposition. Therefore, a stable perovskite layer formed, but the film had a large roughness of 0.67 μm, higher than those observed in spin-dip samples (Table 1). It is also found that, in general, at similar process and fabrication conditions, the surface topography of the film made by
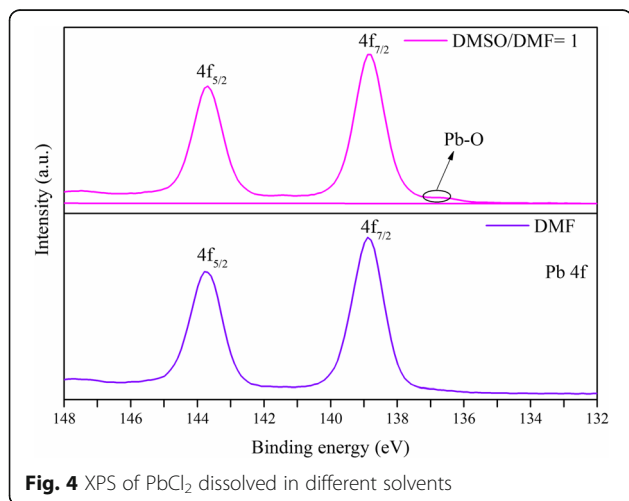
Ahmadian-Yazdi *et al. Nanoscale Research Letters* (2016) 11:408
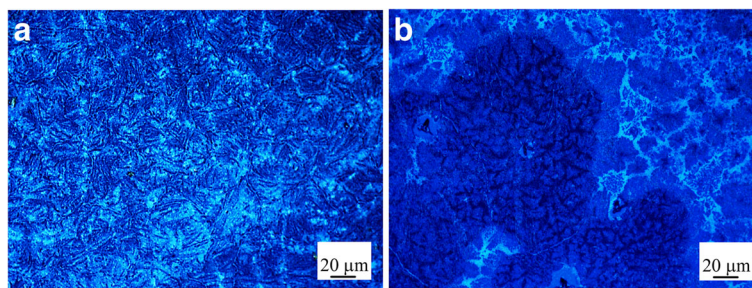
Page 8 of 11

Fig. 5 Optical images on the effect of dipping time on the coverage and morphology of spin-dip perovskites: **a** 90 s (run 9) and **b** 150 s (run 8)

spin-spin coating is similar to the topography of the film made by spin-dip coating (figure not shown). It was also observed that in spin-spin coating, when the MAI solution was spun atop the spun-on $PbCl_2$ thin film, the color changed to dark brown even before annealing, indicating that the perovskite layer had formed. Therefore, perovskite conversion in spin-spin coating is achieved easier than that in spin-dip coating, due to the positive effect of the centrifugal forces that improve mixing of the precursors and therefore lead to better chemical conversion. On the other hand, the presence of the centrifugal forces applied on the wet perovskite film may promote dewetting; nevertheless, by controlling the spin velocity, the dewetted areas and defects may be decreased.

The previous section reveals the difficulties associated with controlling the two-step sequential deposition of perovskite, simply because of the involvement of numerous process parameters. Therefore, in this study, the one-step spin coating was also applied to fabricate perovskite films (run 11). The mixture of perovskite precursors was spun at two spin speeds: first at a low speed (750 rpm for 20 s) to allow nucleation of perovskite crystals, immediately followed by spinning at a higher speed (3000 rpm for 60 s) to complete the film formation process. This one-step method is straightforward and preferred, if desired coverage and conversion can be obtained.

To compare the conversion of precursors to perovskite, the XRD patterns of the best sequential spin-dip (run 1), spin-spin (run 10), and one-step (run 11) spin-coated perovskites are shown in Fig. 6. The background FTO peaks are due to the FTO-coated glass substrate and may be disregarded. The perovskite peaks are observed in all samples. Also, there is no layer of MAI left on the film surfaces as the peaks suggest, indicating effective conversion of MAI to perovskite. The XRD pattern of the sample made by spin-spin coating reveals that the conversion of the precursor solutions to perovskite crystals has increased compared to the spin-dip film of run 1. The film made using the one-step deposition shows the best perovskite conversion, although PbI_2 peaks are not completely removed. Figure 7 shows the absorbance of

the perovskite layers produced by sequential spin-dip and spin-spin coating, as well as one-step spin coating. All films show a drop in the absorbance around the wavelength of 750 nm, which is the characteristic of perovskite layers due to their bandgap, because at large wavelengths, the low-energy photons cannot be absorbed by perovskite. The needle-like structure of the mixed-halide perovskite has been argued to be responsible for good absorbance at low wavelengths, due to internal light scattering of this kind of structure [30]. Although poor coverage of perovskite layer could lead to a decrease in absorbance, this specific structure and the light scattering in the crystals enhances the absorbance. The spin-dip sample prepared based on the conditions of run 1 exhibits the best absorbance in a wide range of wavelengths. The sample made using the one-step spin coating based on the conditions of run 11 shows good absorbance at low wavelengths, but its absorbance declines at wavelengths higher than 550 nm. It is deduced that the spin-dip perovskite is thicker than the one-step spin-coated perovskite, resulting in better absorbance in the spin-dip sample. The dipping process results in the formation of thicker films. In summary, the
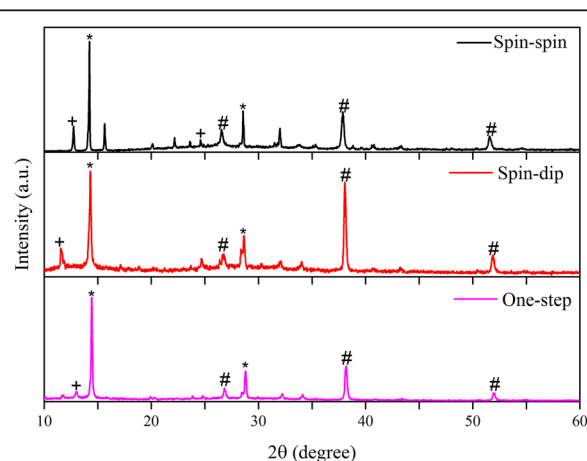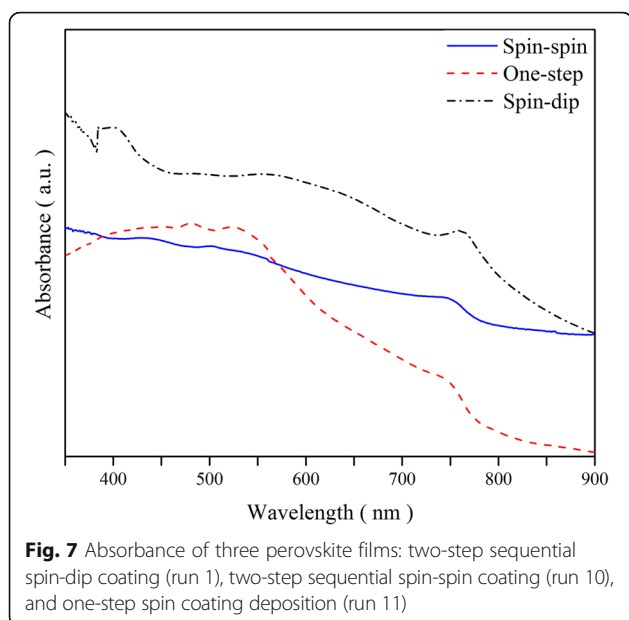

Fig. 6 The XRD patterns of perovskites, deposited by spin-dip (run 1), spin-spin (run 10), and one-step (run 11) methods. The *asterisk* denotes the perovskite peaks, the *number sign* denotes the FTO peaks, and the *plus sign* denotes the PbI_2 peaks

Ahmadian-Yazdi *et al. Nanoscale Research Letters* (2016) 11:408

Page 9 of 11

Fig. 7 Absorbance of three perovskite films: two-step sequential spin-dip coating (run 1), two-step sequential spin-spin coating (run 10), and one-step spin coating deposition (run 11)

Table 2 Photovoltaic performance of devices made by two-step sequential spin-dip (run 1) and one-step deposition

	J_{sc} (mA cm^{-2})	V_{oc} (V)	Fill factor	PCE (%)
Spin-dip (run 1)	12.8	0.63	0.43	3.47
One-step (run 11)	24.38	0.93	0.32	7.26

XRD patterns (c.f. Fig. 6) show the best conversion for the one-step deposition, whereas the absorbance data of Fig. 7 show that the spin-dip sample has a higher absorbance.
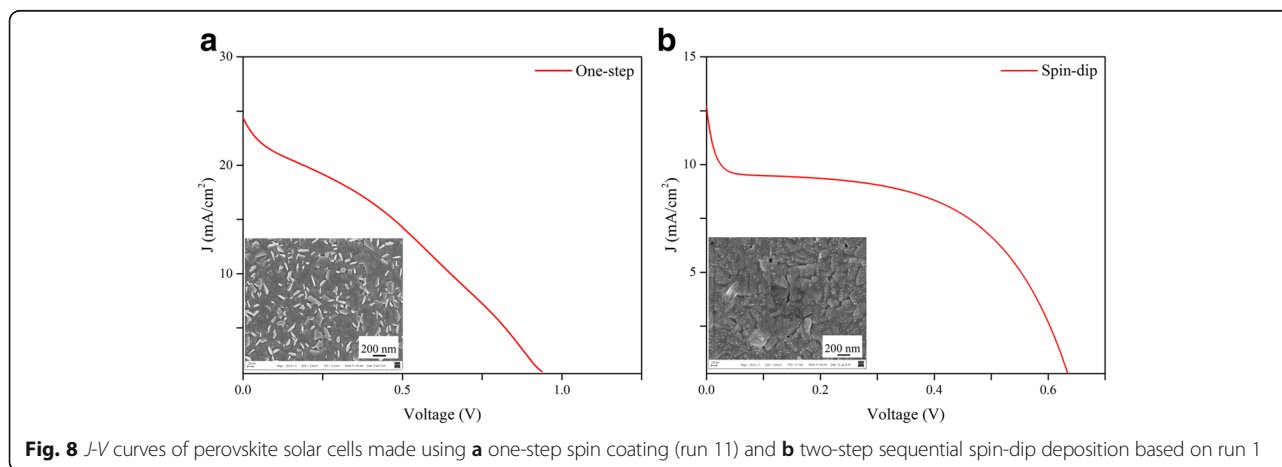
Based on the conclusions of the forgoing fundamental study on the characteristics of perovskites made using one-step and two-step sequential methods, it is inferred that the spin-dip perovskite film made based on run 1 and the perovskite film made based on the one-step spin coating method have the best overall coverage, conversion, and absorbance. Thus, these perovskite films were incorporated into planar perovskite SCs. Figure 8 displays the *J-V* curves and SEM images at the inset showing the coverage, and Table 2 lists the summary of the performance of the fabricated cells. Although the perovskite and other layers were made in a controlled environment in nitrogen-filled glove box, for deposition of electrodes by thermal evaporation, and also for
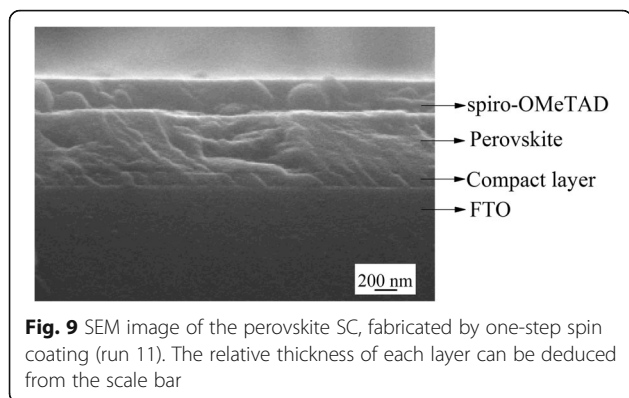
performance tests, the cells were exposed to humid air of Shanghai (relative humidity in Shanghai is higher than 50 % most of the time). It is well known that high humidity is detrimental to the stability and performance of perovskite SCs. Bearing these difficulties in mind, a moderate PCE of 7.26 % for the one-step cell and a PCE of 3.47 % for the spin-dip cell was recorded. The *J-V* curve of the spin-dip device shows anomalous behavior close to the short circuit condition, where the slope of the curve and therefore the shunt resistance changes significantly. Overall, the devices fabricated using the two-step sequential spin-dip coating of run 1 were found rather non-reproducible due to the lack of adequate control on the dipping process. The higher PCE of the one-step cell is attributed to better perovskite conversion, as evidenced from the XRD patterns (c.f. Fig. 6), and better charge collection, even though the absorbance of the one-step perovskite was lower than that of the spin-dip perovskite (c.f. Fig. 7).

Figure 9 shows the SEM cross-sectional image of the cell fabricated using the one-step spin coating method. The thickness of the c-TiO$_2$, perovskite, and spiro-OMeTAD layers are approximately 70, 350, and 200 nm, respectively. The SEM image shows uniform film thickness and good interfaces between adjacent layers. The perovskite thickness of the one-step device is in the ideal range as corroborated by Docampo et al. [31], who obtained the best device performance for perovskite thicknesses in the range of 300–400 nm, enabling the active layer to absorb near 90 % of the incident photons between 350 and 750 nm. Increasing the film thickness to

Fig. 8 *J-V* curves of perovskite solar cells made using **a** one-step spin coating (run 11) and **b** two-step sequential spin-dip deposition based on run 1

Ahmadian-Yazdi *et al. Nanoscale Research Letters* (2016) 11:408

Page 10 of 11

Fig. 9 SEM image of the perovskite SC, fabricated by one-step spin coating (run 11). The relative thickness of each layer can be deduced from the scale bar

600 nm exhibited 99 % light absorbance but caused a drop in the short circuit current. A drop in the short circuit current of the spin-dip device compared to that of the one-step spin-coated device (c.f. Fig. 8) is therefore attributed to the increased thickness of the perovskite layer made by the spin-dip process and/or inadequate perovskite conversion. In summary, we found that the one-step fabrication method is preferred, due to the ease of fabrication, better control on the process, fewer parameters to control, and higher device performance and reproducibility.

Conclusions

In this work, the characteristics of two-step sequential spin-dip- and spin-spin-coated, as well as one-step spin-coated, mixed-halide perovskite films were studied. In particular, in the spin-dip method, the effect of annealing temperature, choice of solvent for $PbCl_2$, dipping time, and spin velocity on the surface topography and roughness, conversion of precursor solutions to perovskite crystals, and light absorbance was studied. Planar devices based on the FTO-coated glass/c-TiO_2/perovskite/spiro-OMeTAD/Ag structure were fabricated using two-step spin-dip and one-step spin coating methods.

It was found that higher annealing temperature (160 °C) produces a more uniform perovskite film compared to a lower temperature (100 °C). However, high temperature may result in sintering of perovskite crystals. Therefore, within the range of the temperatures studied here, an annealing temperature of 100 °C was found to be the optimum annealing temperature for the best overall performance. Two types of dewetting in perovskite films were observed and discussed in this work. These include dewetting due to the growth of perovskite crystals (crystallization dewetting) and dewetting due to the growth of perturbations in thin liquid films, originating from the intermolecular forces (spinodal dewetting) or impurities (heterogeneous nucleation). It was found that at high spin speeds, the film becomes ultrathin and

dewets. The critical spin speed for dewetting depends on spin time and solution physical properties, as well.

The effect of the choice of solvent on $PbCl_2$ film was studied, where it was found that a mixture of DMF and DMSO at a comparable volume ratio favors the formation of a film with high coverage. The XRD data showed that the perovskite film deposited using the one-step deposition shows the highest conversion of precursors to perovskite, whereas the film made using the two-step sequential spin-dip coating exhibited the highest absorbance. The device fabricated using the one-step method showed a PCE of 7.6 %, whereas the device made using the sequential spin-dip coating showed a PCE of 3.45 % but a higher fill factor. The SEM cross-sectional image of the one-step spin-coated cell showed excellent interfaces between the adjacent layers. However, during some steps of fabrication and testing, the devices were exposed to humid air (~50 %) and thus showed limited performance, showing the strong effect of humidity on perovskite solar cells.

Authors' contributions
MRAY performed the experiments and characterization tests and fabricated the solar cells. FZ contributed to device fabrication, improvement of device performance, data analysis and interpretations. MH assisted with the device fabrication. All authors contributed to the discussion of the data and preparation and writing of the manuscript. ME directed the work. All authors read and approved the final manuscript.

Competing interests
The authors declare that they have no competing interests.

References
1. NREL Efficiency Chart. http://www.nrel.gov/ncpv/images/efficiency_chart.jpg. Accessed June 2016
2. Habibi M, Zabihi F, Ahmadian-Yazdi MR, Eslamian M (2016) Progress in emerging solution-processed thin film solar cells—part II: perovskite solar cells. Renew Sust Energ Rev 62:1012–1031
3. Ding Y, Yao X, Zahang X, Wei C, Zhao Y (2014) Surfactant enhanced surface coverage of $CH_3NH_3PbI_{3-x}Cl_x$ perovskite for highly efficient mesoscopic solar cells. J Power Sources 272:351–355
4. Kojima A, Teshima K, Shirai Y, Miyasaka T (2009) Organometal halide perovskites as visible-light sensitizers for photovoltaic cells. J Am Chem Soc 131:6050–6051
5. Chen Q, Zhou H, Hong Z, Luo S, Duan HS, Wang HH, Liu Y, Li G, Yang Y (2014) Planar heterojunction perovskite solar cells via vapor-assisted solution process. J Am Chem Soc 136:622–625
6. Noel NK, Stranks SD, Abate A, Wehrenfennig C, Guarnera S, Haghighirad AA, Sadhanala A, Eperon GE, Pathak SK, Johnston MB, Petrozza A, Herz LM, Snaith HJ (2014) Lead-free organic–inorganic tin halide perovskites for photovoltaic applications. Energy Environ Sci 7:3061
7. Stranks SD, Giulia Grancini GEE, Menelaou C, Alcocer MJP, Leijtens T, Herz LM, Petrozza A, Snaith HJ (2013) Electron–hole diffusion lengths exceeding 1 micrometer in an organometal trihalide perovskite absorber. Science 342:341–344

Ahmadian-Yazdi *et al. Nanoscale Research Letters* (2016) 11:408

Page 11 of 11

8.   Wehrenfennig C, Eperon GE, Johnston MB, Snaith HJ, Herz LM (2014) High charge carrier mobilities and lifetimes in organolead trihalide perovskites. Adv Mater 26:1584–1589

9.   Wang K, Shi Y, Dong Q, Li Y, Wang S, Yu X, Wu M, Ma T (2015) Low-temperature and solution-processed amorphous WOX as electron-selective layer for perovskite solar cells. J Phys Chem Lett 6:755–759

10. Zhao Y, Zhu K (2014) Solution chemistry engineering toward high-efficiency perovskite solar cells. J Phys Chem Lett 5:4175–4186

11. You J, Hong Z, Yang YM, Chen Q, Cai M, Song TB, Chen CC, Lu S, Liu Y, Zhou H, Yang Y (2014) Low-temperature solution-processed perovskite solar cells with high efficiency and flexibility. ACS Nano 8:1674–1680

12. Barrows AT, Pearson AJ, Kwak CK, Dunbar ADF, Buckley AR, Lidzey DG (2014) Efficient planar heterojunction mixed-halide perovskite solar cells deposited via spray-deposition. Energy Environ Sci 7:2944

13. Zhang LQ, Zhang XW, Yin ZG, Jiang Q, Liu X, Meng JH, Zhao YJ, Wang HL (2015) Highly efficient and stable planar heterojunction perovskite solar cells via a low temperature solution process. J Mater Chem A 3:12133–12138

14. Chen Y, Chen T, Dai L (2015) Layer-by-layer growth of CH(3)NH(3)PbI(3-x)Clx for highly efficient planar heterojunction perovskite solar cells. Adv Mater 27:1053–1059

15. Kim JH, Williams ST, Cho N, Chueh CC, Jen AKY (2014) Enhanced environmental stability of planar heterojunction perovskite solar cells based on blade-coating. Adv Energy Mater 5:1401229. doi:10.1002/aenm.201401229

16. Zabihi F, Ahmadian-Yazdi MR, Eslamian M (2016) Fundamental study on the fabrication of inverted planar perovskite solar cells using two-step sequential substrate vibration-assisted spray coating (2S-SVASC). Nanoscale Res Lett 11:71

17. Qin P, Tanaka S, Ito S, Tetreault N, Manabe K, Nishino H, Nazeeruddin MK, Gratzel M (2014) Inorganic hole conductor-based lead halide perovskite solar cells with 12.4 % conversion efficiency. Nat Commun 5:3834

18. Burschka J, Pellet N, Moon SJ, Humphry-Baker R, Gao P, Nazeeruddin MK, Gratzel M (2013) Sequential deposition as a route to high-performance perovskite-sensitized solar cells. Nature 499:316–319

19. Eslamian M, Zabihi F (2015) Ultrasonic substrate vibration-assisted drop casting (SVADC) for the fabrication of photovoltaic solar cell arrays and thin-film devices. Nanoscale Res Lett 10:462

20. Zheng L, Ma Y, Chu S, Wang S, Qu B, Xiao L, Chen Z, Gong Q, Wu Z, Hou X (2014) Improved light absorption and charge transport for perovskite solar cells with rough interfaces by sequential deposition. Nanoscale 6:8171–8176

21. Choi JJ, Yang X, Norman ZM, Billinge SJ, Owen JS (2014) Structure of methylammonium lead iodide within mesoporous titanium dioxide: active material in high-performance perovskite solar cells. Nano Lett 14:127–133

22. Eperon GE, Burlakov VM, Docampo P, Goriely A, Snaith HJ (2014) Morphological control for high performance, solution-processed planar heterojunction perovskite solar cells. Adv Funct Mater 24:151–157

23. Zabihi F, Xie Y, Gao S, Eslamian M (2015) Morphology, conductivity, and wetting characteristics of PEDOT:PSS thin films deposited by spin and spray coating. Appl Surf Sci 338:163–177

24. Habibi M, Rahimzadeh A, Eslamian M (2016) On dewetting of thin films due to crystallization (crystallization dewetting). Eur Phys J E Soft Matter 39:30

25. Jeon NJ, Noh JH, Kim YC, Ryu S, Yang WS, Seok SI (2014) Solvent engineering for high-performance inorganic–organic hybrid perovskite solar cells. Nat Mater 13:897–903

26. Raga SR, Jung MC, Lee MV, Leyden MR, Kato Y, Qi Y (2015) Influence of air annealing on high efficiency planar structure perovskite solar cells. Chem Mater 27:1597–1603

27. Ng TW, Chan CY, Lo MF, Guan ZG, Lee CS (2015) Formation chemistry of perovskites with mixed iodide/chloride content and the implications on charge transport properties. J Mater Chem A 3:9081–9085

28. Li W, Fan J, Li J, Mai Y, Wang L (2015) Controllable grain morphology of perovskite absorber film by molecular self-assembly toward efficient solar cell exceeding 17 %. J Am Chem Soc 137:10399–10405

29. Yu H, Wang F, Xie F, Li W, Chen J, Zhao N (2014) The role of chlorine in the formation process of "$CH_3NH_3PbI_{3-x}Cl_x$" perovskite. Adv Funct Mater 24: 7102–7108

30. Conings B, Baeten L, De DC, D'Haen J, Manca J, Boyen HG (2014) Perovskite-based hybrid solar cells exceeding 10 % efficiency with high reproducibility using a thin film sandwich approach. Adv Mater 26:2041–2046

31. Docampo P, Ball JM, Darwich M, Eperon GE, Snaith HJ (2013) Efficient organometal trihalide perovskite planar-heterojunction solar cells on flexible polymer substrates. Nat Commun 4:2761